*Egypt. J. Chem.* **Vol. 68,** SI: Z. M. Nofal, pp. 15 - 28 (2025)

**Egyptian Journal of Chemistry**

**http://ejchem.journals.ekb.eg/**

# A Novel Functionalized Metal-Organic Framework for Sensitive Detection and Efficient Removal of Manganese Ions from Drinking Water

**Mohamed Hosni[1]*, Reda M Abd El-aal[2], Ahmed Shahat[2], Islam M. El-Sewify[3]**

[1]*Center for Applied Research on the Environment and Sustainability, The American University in Cairo, 11835 Cairo, Egypt*

[2]*Department of Chemistry, Faculty of Science, Suez University,43518, Suez, Egypt*

[3]*Department of Chemistry, Faculty of Science, Ain Shams University, 11566 Cairo, Abbassia, Egypt*

**Abstract**

Manganese nano sensor (MNS) derived from Al-$NH_2$-MIL-53(ANM-53) via Schiff base condensation with 1-hydroxy-2-naphthaldehyde exhibits exceptional sensing capabilities for $Mn^{2+}$ ions in aqueous media. This study presents a comprehensive investigation into the synthesis, characterization, and application of MNS as both a chemical sensor and adsorbent for manganese ions, which are environmentally concerning contaminants in drinking water systems. The functionalized MOF demonstrates remarkable sensitivity with a detection limit of 0.61 ppb, with a linear range from 0.005 to 0.01 ppm, outperforming many conventional sensing methodologies. The sensing mechanism is mediated by coordination interactions between the Schiff base moieties and $Mn^{2+}$ ions, resulting in measurable spectroscopic shifts. FTIR, SEM, TEM, XRD, and BET analyses confirm the successful functionalization while maintaining the structural integrity and porosity of the parent framework. The MNS material simultaneously functions as an effective adsorbent, removing up to 92% of $Mn^{2+}$ ions from aqueous solutions within 120 seconds under optimized conditions. This dual-functional nanomaterial presents a promising platform for both monitoring and remediating manganese contamination in water resources, addressing a critical environmental and public health concern with potential applications in portable water quality monitoring devices.

***Keywords:*** Metal-organic framework; Manganese detection; Chemical sensor; Water treatment; Schiff base functionalization; Environmental monitoring; Toxic metal remediation

## 1. Introduction

Manganese (Mn) represents a vital micronutrient for metabolic processes in plants and animals but becomes hazardous when present at elevated concentrations in environmental matrices. Despite its ubiquity and importance as a trace element [1-5], manganese contamination in water systems remains an underreported environmental concern with significant public health implications. The anthropogenic release of manganese into aquatic ecosystems has accelerated through industrial processes, mining operations, and agricultural activities [6-7]. Manganese pollution in water systems presents multifaceted environmental and health concerns. Manganese contamination in drinking water arises from natural geological leaching and anthropogenic activities, with groundwater sources particularly susceptible due to prolonged rock-water interactions. While essential in trace amounts, chronic exposure to elevated manganese levels (>100 ppb) correlates with neurotoxic effects in children and Parkinson-like symptoms in adults, driving contentious revisions of international guidelines. Groundwater systems globally report manganese concentrations exceeding 400 ppb in vulnerable aquifers, complicating regulatory efforts to balance aesthetic concerns (staining, taste) with emerging neurological health risks [2,4,8,9]. Human health implications of manganese overexposure are particularly concerning. When accidentally inhaled or ingested, manganese can bypass normal physiological barriers, directly affecting neurological systems [6,10]. Studies have demonstrated that manganese disrupts dopamine, serotonin, and glutamine signaling in the brain, potentially leading to manganism, a debilitating neurodegenerative disorder [11-14]. The current World

*Corresponding author e-mail: mohamed_hosni@aucegypt.edu.; (**Mohamed Hosni Ramadan**).
Received date 29 April 2025; Revised date 03 June 2025; Accepted date 28 June 2025
DOI: 10.21608/EJCHEM.2025.380150.11669

Health Organization guideline for manganese in drinking water is 0.4 mg/L (400 ppb) [15]. However, evidence suggests neurological effects may occur at concentrations below this threshold, particularly in vulnerable populations such as children and the elderly [15-17]. Traditional approaches for manganese detection and removal include atomic absorption spectroscopy [18], inductively coupled plasma mass spectrometry [19], and conventional adsorption using activated carbon or ion exchange resins [20-22]. While effective, these methodologies often require sophisticated instrumentation, technical expertise, and significant operational costs that limit their widespread implementation. This technological gap has driven research interest toward developing multifunctional materials capable of simultaneously detecting and removing manganese from water systems with high sensitivity and selectivity [23]. Metal-organic frameworks (MOFs) have emerged as exceptional candidates for chemical sensing and environmental remediation applications due to their unique structural and chemical properties [24-25]. These crystalline porous materials, composed of metal ions or clusters coordinated to organic ligands, offer unprecedented surface areas, tunable pore architectures, and diverse chemical functionalities that can be strategically engineered for specific applications, which makes MOFs particularly well-suited for chemical sensing applications targeting various analytes [24-26]. The versatility of MOFs as sensing platforms is further enhanced by their modularity, allowing for the incorporation of functional groups through direct synthesis or post-synthetic modification [24-30]. Recent advances in MOF chemistry have demonstrated particular promise in the detection and removal of heavy metals from water systems. MOF-based sensors employing various transduction mechanisms—electrical, optical, and electrochemical—have shown remarkable sensitivity toward metal ions, with detection limits reaching parts-per-billion levels. Simultaneously, the high surface area and abundant coordination sites within MOF structures facilitate efficient adsorption and removal of metal contaminants, presenting opportunities for dual-function materials that both sense and sequester environmental pollutants [24-30]. The integration of Schiff base chemistry with MOF platforms represents a particularly promising approach for metal ion sensing and capture. Schiff bases, formed through the condensation of primary amines with carbonyl compounds, offer excellent metal-coordination properties through their N, O-donor atoms. The condensation of primary amines in the MOF structure with aldehydes such as 1-hydroxy-2-naphthaldehyde produces Schiff bases with excellent ability and enabling selective interactions with transition metal ions such as manganese. When incorporated into MOF structures, these functional groups can create highly specific binding pockets for target metal ions, inducing measurable changes in optical or electronic properties that serve as the basis for sensing applications [24-32]. MOFs have emerged as versatile platforms for ion sensing, though their application for manganese detection remains underexplored compared to other heavy metals [1,2]. Recent studies demonstrate Mn-based MOFs as effective sensors for nitrite ions and $d^{10}$ metals like $Ag^{+}$/$Cd^{2+}$ through fluorescence modulation [33,34], while Mn-MOF/carbon composites show enhanced electrochemical sensing capabilities [35]. The paramagnetic nature of $Mn^{2+}$ poses challenges for selective detection due to fluorescence quenching effects, yet structural tunability of MOFs offers potential for tailored recognition sites [36]. Current research highlights MOFs' dual functionality in sensing and adsorption, with Mn-MOFs exhibiting unique solvent-dependent luminescence properties that could be adapted for manganese-specific detection. These developments underscore MOFs' promise for addressing manganese monitoring needs in environmental and biological systems through innovative design strategies [37]. In this context, the amino-functionalized MOF Al-$NH_2$-MIL-53 presents an attractive platform for developing manganese-specific sensors and adsorbents. The inherent structural flexibility of the MIL-53 topology, characterized by its "breathing" behavior in response to guest molecules, combined with the reactive amino groups suitable for post-synthetic modification, provides an ideal foundation for creating functionalized materials with enhanced sensitivity and selectivity toward manganese ions. In this study, we report the synthesis and characterization of a novel manganese nano sensor (MNS) derived from Al-$NH_2$-MIL-53(ANM-53) through Schiff base condensation with 1-hydroxy-2-naphthaldehyde. The resulting material demonstrates exceptional capabilities for detection and efficient removal of $Mn^{2+}$ ions from aqueous solutions with an excellent limit of detection (LOD) of 0.61 ppb, which is way lower than the allowable manganese level in tap water (400 ppb). We investigate the structural properties, sensing mechanism, and adsorption performance of MNS through various analytical techniques, including FTIR, UV-vis spectroscopy, X-ray diffraction (XRD), and Brunauer-Emmett-Teller (BET) analysis. The practical utility of MNS for real-world applications is evaluated through performance comparisons

with existing technologies, establishing its potential as a multifunctional platform for addressing manganese contamination in water resources.

## 2. Materials and Methods

### Chemicals and Reagents

All reagents utilized in this study were of analytical grade and employed without further purification to ensure experimental reproducibility and material integrity. Aluminum chloride hexahydrate ($AlCl_3 \cdot 6H_2O$, 98%), 2-aminoterephthalic acid ($NH_2$-$H_2BDC$, 99%), 1-hydroxy-2-naphthaldehyde (98%), N, N-dimethylformamide (DMF, 99.8%), methanol ($CH_3OH$, 99.9%), and ethanol ($C_2H_5OH$, 99.5%) were purchased from Sigma-Aldrich (Germany) and used as received. Deionized water (resistivity 18.2 MΩ·cm) produced by a Milli-Q water purification system (Millipore, USA) was used for all aqueous solutions.

For the UV-Vis and interference, and selectivity studies, certified single-element standard solutions (1000 mg/L) of various manganese and metal ions were acquired from Merck (Germany). These standards were appropriately diluted with deionized water to the required concentrations prior to use. All experimental glassware and plasticware were rigorously cleaned by soaking in 10% nitric acid, followed by thorough rinsing with deionized water to eliminate any potential contamination.

### Synthesis of Al-$NH_2$-MIL-53 (ANM-53)

The amino-functionalized metal-organic framework ANM-53 was synthesized following a modified solvothermal procedure [38] (**Scheme 1.**). Briefly, 0.838 g of aluminum chloride (5.54 mmol) and 1.00 g of 2-aminoterephthalic acid (5.52 mmol) were dissolved in 30 mL of DMF in a 100 mL Teflon-lined stainless-steel autoclave. The mixture was sonicated for 15 minutes to ensure complete dissolution and then heated at 150°C for 8 hours. After cooling to room temperature naturally, the resulting yellow precipitate was collected by centrifugation and washed thoroughly with fresh DMF (3 × 30 mL) to remove unreacted starting materials. The as-synthesized material, denoted as ANM-53(as), was then subjected to a two-step activation process to remove guest molecules and open the porous structure. First, the material was immersed in DMF at 150°C for 24 hours to obtain ANM-53(DMF). Subsequently, the solvent was exchanged with methanol (3 × 30 mL) at room temperature over 24 hours. The methanol-exchanged solid was then heated at 130°C under vacuum for 12 hours to remove the solvent molecules, yielding the activated ANM-53 material.

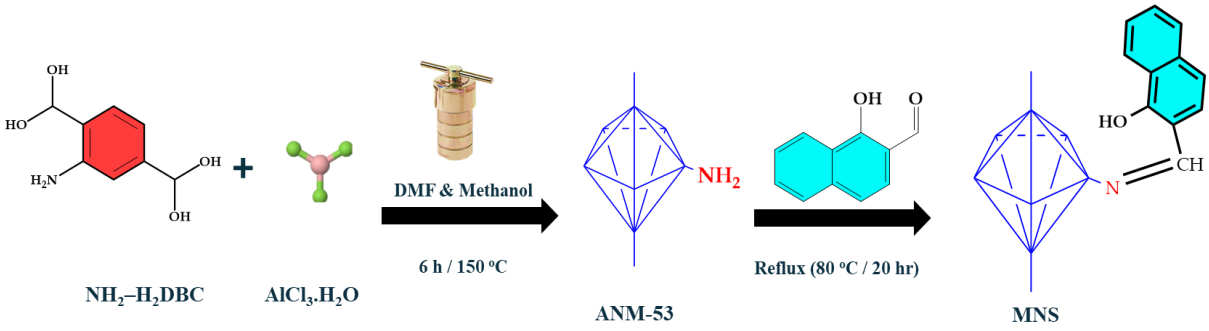


**Scheme 1.** Schematic representation for the synthesis of ANM-53 and MNS materials

### Preparation of Manganese Nano Sensor (MNS)

MNS was prepared through post-synthetic modification of ANM-53 via Schiff base condensation with 1-hydroxy-2-naphthaldehyde (**Scheme 1.**). In a typical procedure, 1.0 g of activated ANM-53 was dispersed in 50 mL of anhydrous ethanol in a 100 mL round-bottom flask. To this suspension, 0.86 g of 1-hydroxy-2-naphthaldehyde (5.0 mmol) was added, and the mixture was refluxed at 65°C for 24 hours. The resulting orange-yellow solid was collected by filtration, washed extensively with methanol (5 × 30 mL) to remove excess aldehyde, and then dried under vacuum at 80°C for 12 hours to obtain the MNS material.

**Characterization Techniques**

X-ray powder diffraction (XRD) patterns of the synthesized materials were recorded on a diffractometer using Cu Kα radiation (λ = 1.5418 Å) at 40 kV and 40 mA in the 2θ range of 5-50° with a step size of 0.02°. Nitrogen adsorption-desorption isotherms were measured at 77 K using a surface area analyzer. Prior to measurements, samples were degassed at 120°C for 12 hours under vacuum. Specific surface areas were calculated using the BET method, while pore size distributions were determined by the Barrett-Joyner-Halenda (BJH) method. Fourier transform infrared (FTIR) spectra were recorded on a spectrophotometer using KBr pellets in the range of 4000-400 $cm^{-1}$ with a resolution of 4 $cm^{-1}$. UV-visible absorption spectra were measured using a double-beam spectrophotometer with a 1 cm quartz cuvette in the wavelength range of 200-800 nm. Scanning electron microscopy (SEM) images were obtained using an electron microscope operating at an acceleration voltage of 15 kV. Prior to imaging, samples were sputter-coated with a thin layer of gold.

**Evaluation of MNS material for the sensing of $Mn^{2+}$ ions**

The sensing capability of MNS toward $Mn^{2+}$ ions was evaluated using UV-visible spectroscopy. A stock solution of $Mn^{2+}$ (1000 ppm) was diluted with deionized water. Working solutions with different $Mn^{2+}$ concentrations (0.0005-1.0 ppm) were prepared by serial dilution of the stock solution.

For UV-vis measurements, 10 mg of MNS was dispersed in 10 mL of aqueous solution containing different concentrations of $Mn^{2+}$ ions. The suspensions were sonicated for 30 seconds and then stirred for 3 minutes at room temperature to ensure adequate interaction between the sensor and analyte. The supernatants were used, and their absorption spectra were recorded in the range of 200-800 nm. The effect of pH on the sensing performance was investigated by adjusting the pH of the $Mn^{2+}$ solutions (0.1 ppm) from 2 to 10 using buffer solutions before adding the MNS material. The response time of the sensor was determined by monitoring the absorbance change over time after adding MNS to the $Mn^{2+}$ solution (0.1 ppm).

**$Mn^{2+}$ Removal Experiments from Drinking Water**

Batch adsorption experiments were conducted to evaluate the $Mn^{2+}$ ions removal efficiency of MNS from drinking water. Typically, 10 mg of MNS was added to 50 mL of drinking water mixed with $Mn^{2+}$ with initial concentrations ranging from 1 to 100 ppm. The mixtures were stirred at 200 rpm at room temperature (25 ± 1°C) for predetermined time intervals of 30 minutes. After centrifugation, the residual $Mn^{2+}$- MNS' material was removed through filtration, and drinking water samples were analyzed with AAS before and after treatment with the MNS material.

## 3. Results and Discussion

**Structural Characterization**

**Figure 1** presents the infrared spectral comparison between ANM-53 and the MNS. Spectroscopic analysis reveals characteristic amino group absorption bands at 3498 and 3385 $cm^{-1}$, corresponding to asymmetric and symmetric N-H stretching vibrations in ANM-53. These same spectral features appear in the MNS but with diminished intensities, which can be attributed to the partial consumption of amino groups during imine bond formation between ANM-53 and the 1-hydroxy-2-naphthaldehyde molecules.

The carboxylate functional groups manifest through distinctive absorption bands at 1579 $cm^{-1}$ (asymmetric $COO^-$ stretching) and 1435 $cm^{-1}$ (symmetric $COO^-$ stretching). Aromatic framework components are evidenced by C=C stretching vibrations at 1497 and 1401 $cm^{-1}$. Both materials exhibit an absorption signal at approximately 1259 $cm^{-1}$, likely originating from C-N vibrational modes. The spectral region between 1000-1100 $cm^{-1}$ features two distinct Al-O absorption bands, confirming the coordination between aluminum and oxygen atoms within the ANM-53 structure. A significant differentiating feature between the two materials is the presence of an N-H bending (scissoring) vibration at 1685 $cm^{-1}$ in the ANM-53 spectrum, which is notably altered in the functionalized sensor due to the Schiff base condensation reaction and formation of C=N stretching).

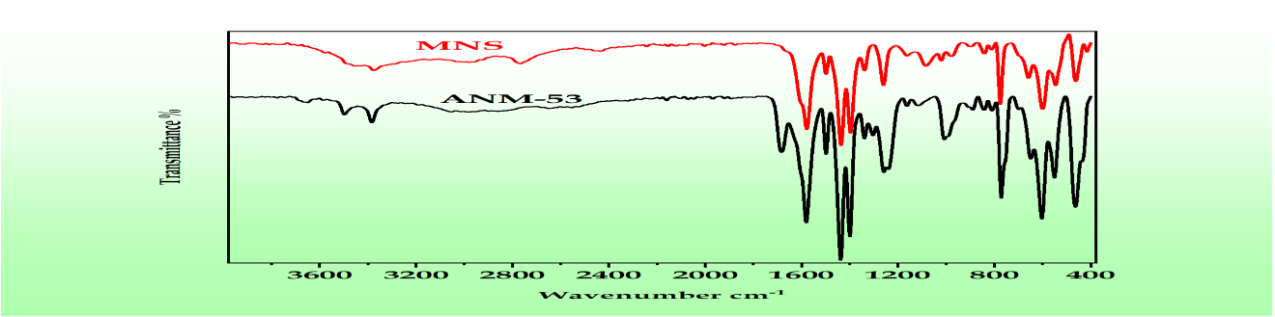


**Figure 1.** FTIR spectra of ANM-53 and MNS.

The successful synthesis of ANM-53 and its modification to create the manganese nano sensor (MNS) were confirmed through various characterization techniques. X-ray diffraction (XRD) patterns of both materials are presented in **Figure 2A**, providing critical insights into their crystalline structures. The XRD pattern of ANM-53 shows characteristic diffraction peaks at 2θ values of approximately 10.22°, 12.53°, 17.44°, 19.84°, 22.77°,24.58°, 26.68°, 29.85°, and 34.92°, which are consistent with the orthorhombic structure of the MIL-53 topology reported in the literature. The well-defined and intense diffraction peaks indicate the high crystallinity of the synthesized material. After Schiff base condensation with 1-hydroxy-2-naphthaldehyde to form MNS, the primary diffraction peaks are preserved, confirming that the fundamental MOF structure remains intact throughout the modification process. However, subtle changes in peak positions and relative intensities are observed, which can be attributed to the incorporation of the bulky naphthaldehyde moieties within the framework. The slight peak broadening in the MNS pattern suggests a minor decrease in crystallinity compared to the parent material, which is commonly observed in post-synthetic modification processes due to the introduction of structural strain. Importantly, the absence of new diffraction peaks indicates that the modification occurs within the framework without forming secondary crystalline phases.

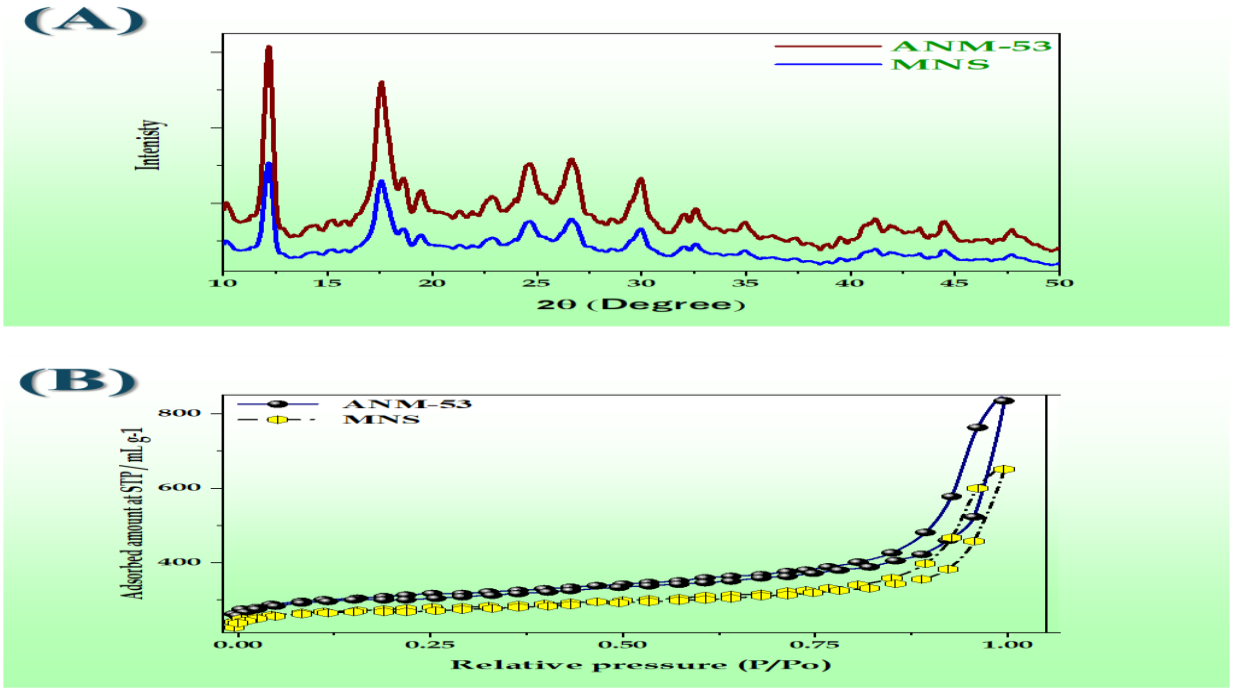


**Figure 2.** (A) PXRD patterns of ANM-53 and MNS confirming structural integrity post-functionalization, with reduced peak intensity in MNS due to Schiff base incorporation. (B) $N_2$ adsorption–desorption isotherms showing decreased surface area and pore volume in MNS, indicating partial pore occupation while preserving mesoporosity.

The textural properties of the parent ANM-53 and the functionalized manganese nanosensor (MNS) were assessed by nitrogen adsorption–desorption isotherm measurements at 77 K, as illustrated in **Figure 2B**. Both materials exhibited typical Type IV isotherms with pronounced hysteresis loops at relative pressures ($P/P_0$) between 0.8 and 1.0, characteristic of mesoporous structures according to the IUPAC classification. Nitrogen adsorption–desorption measurements were conducted at 77 K to evaluate the textural properties of ANM-53 and MNS, with the resulting isotherms shown in **Figure 2B**. Both materials displayed type IV isotherms with H3-type hysteresis loops, characteristic of mesoporous frameworks. The pristine ANM-53 exhibited a high BET surface area of 798 $m^2/g$, which decreased to 604 $m^2/g$ for MNS following Schiff base functionalization. This reduction reflects partial pore blocking by the anchored 1-hydroxy-2-naphthaldehyde ligands. Consistently, the total pore volume decreased from 0.78 $m^2/g$ (ANM-53) to 0.56 $m^2/g$ (MNS). These changes confirm the successful immobilization of functional groups within the mesopores, while the preservation of the isotherm shape and significant porosity indicates that the framework's structural integrity was largely maintained. Despite the reduction, the MNS material retained the characteristic mesoporosity of the parent MOF, maintaining sufficient accessible pore space essential for its dual roles as a sensor and adsorbent. The slight reduction in surface area and pore volume is attributed to successful condensation with the Schiff base moieties within the framework, which, while partially occupying the pore channels, introduces active sites for $Mn^{2+}$ binding. This structural modification is crucial for enhancing selective recognition and adsorption of manganese ions without compromising the overall integrity of the MOF scaffold. SEM images **Figure 3(A)** and **(B)** at 10,000× magnification illustrate that both the original ANM-53 and its Schiff base-functionalized form, MNS, exhibit a closely packed nanostructured surface morphology. The ANM-53 sample appears as a densely packed array of nanoscale crystallites forming a continuous textured surface, and MNS retains this overall arrangement after functionalization. However, MNS shows a slightly rougher surface texture and minor particle aggregation compared to pristine ANM-53, indicating that the introduction of Schiff base ligands induces only subtle textural changes. Likewise, TEM images **(C)** and (D) reveal that both ANM-53 and MNS consist of well-defined, block-like crystalline particles on the sub-micron scale. The functionalized MNS sample preserves the same crystallite shape and size as the parent ANM-53, demonstrating that the Schiff base modification does not significantly alter the core structure or dimensions of the particles. Only slight morphological differences are observed in MNS – such as marginally rougher particle edges or a mild tendency for crystallites to aggregate – but overall the structural integrity and crystallinity are largely preserved after modification. Crucially, this preservation of morphology indicates a successful, non-destructive functionalization that leaves the material's framework intact.

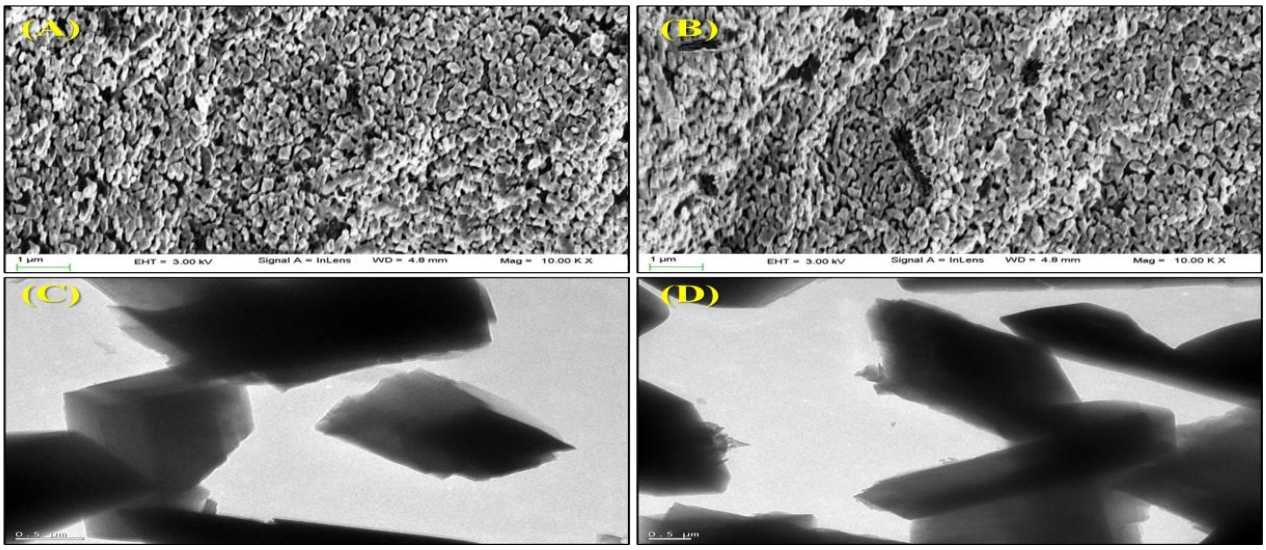


**Figure 3.** SEM and TEM images of (A, C) ANM-53 and (B, D) MNS. SEM micrographs (A, B) show dense nanostructures, while TEM images (C, D) reveal block-like crystallites.

**Effect of Optimization Parameters on MNS Performance**

**Effect of Temperature**

The influence of temperature on the sensing response of MNS toward $Mn^{2+}$ ions was systematically investigated in the range of 5–40 °C, and the results are presented in **Figure 4A**. A progressive enhancement in signal response (%) was observed with an increasing temperature up to 25 °C, beyond which the response plateaued near 100%.

At lower temperatures (5–15 °C), the sensing efficiency was notably suppressed, likely due to reduced diffusion kinetics of $Mn^{2+}$ ions and slower coordination dynamics with the Schiff base functional groups immobilized within the MNS framework. As the temperature increased to 20–25 °C, the signal response sharply improved, reaching approximately 95%, indicating accelerated ion transport and enhanced interaction rates between $Mn^{2+}$ and the active binding sites.

Further elevation of temperature beyond 25 °C up to 40 °C resulted in a saturation of the sensing signal, suggesting that the binding interactions had reached equilibrium, and that additional thermal activation did not contribute significantly to further enhancement. Importantly, the stable high signal across a broad temperature window (25–40 °C) underscores the robustness of MNS under typical environmental and operational conditions.

These findings imply that ambient to mildly elevated temperatures are optimal for achieving maximal sensing performance, making MNS a viable candidate for practical field applications where temperature variations are expected.

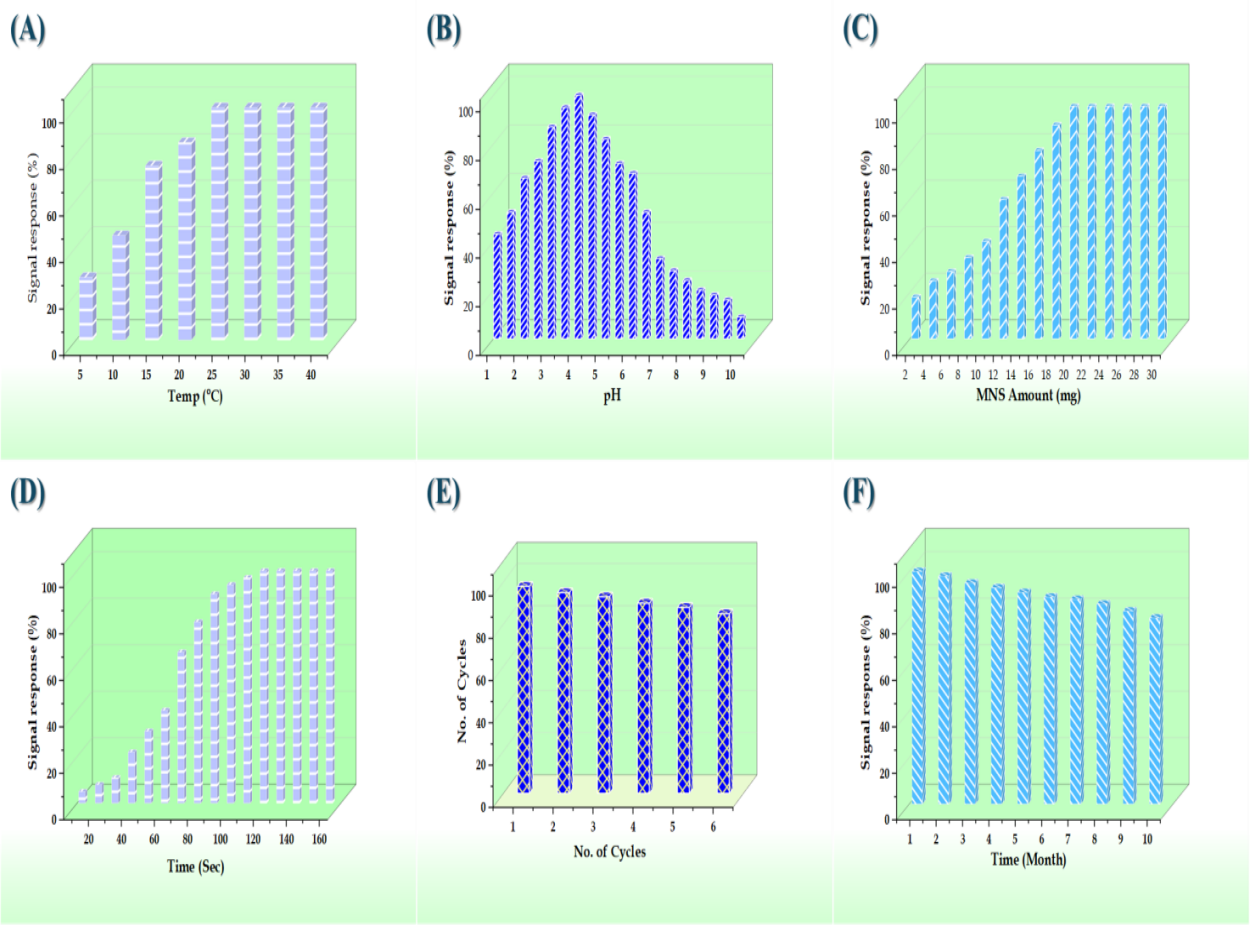


**Figure 4.** Optimization and performance evaluation of MNS for $Mn^{2+}$ detection: (A) Effect of temperature on signal response, showing optimal performance at 25 °C. (B) pH-dependent sensing behavior with maximum response at pH 4.0. (C) Influence of MNS dosage, indicating saturation at ~20 mg. (D) Response kinetics showing rapid signal development within 120 s. (E) Reusability over six cycles demonstrates high retention of sensing efficiency. (F) Long-term stability of MNS over 10 months with minimal signal loss

**Effect of pH**

The pH of the solution plays a crucial role in determining the sensing performance of the MNS material. The effect of pH on $Mn^{2+}$ detection was systematically investigated by measuring the absorbance response in buffer solutions ranging from pH 1 to 10. As shown in **Figure 4B**, the MNS sensor exhibits maximum sensitivity in the pH range of 3.5 - 4, with a significant decrease in response observed at pH values above 7. The enhanced sensitivity at acidic pH can be attributed to the protonation-deprotonation equilibrium of the Schiff base moieties derived from 1-hydroxy-2-naphthaldehyde.

At lower pH values (< 3), the reduced response is likely due to competition between $H^+$ and $Mn^{2+}$ ions for binding sites, while at higher pH values (> 7), the formation of $Mn(OH)_2$ precipitates can interfere with the sensing mechanism. Additionally, deprotonation of the phenolic hydroxyl groups at alkaline pH alters the electronic structure of the binding sites, reducing their affinity for $Mn^{2+}$ ions. The findings revealed that at pH 4.0, the phenolic –OH group is partially deprotonated, enabling coordination with $Mn^{2+}$ ions. Therefore, all subsequent sensing experiments were conducted at the optimal pH of 4.0.

**Effect of MNS Amount**

The amount of sensing material used in detection is a critical parameter affecting both sensitivity and cost-effectiveness. The influence of MNS dosage on $Mn^{2+}$ detection was investigated by varying the amount of MNS from 1 to 10 mg per 10 mL of test solution while maintaining a constant $Mn^{2+}$ concentration (0.1 ppm). As illustrated in **Figure 4C**, the absorbance intensity increased proportionally with increasing MNS dosage from 2 to 20 mg, beyond which the response plateaued.

The observed saturation effect at higher MNS dosages can be attributed to the limited number of $Mn^{2+}$ ions available in the solution. An optimal MNS dosage of 20 mg per 10 mL was selected for subsequent experiments, providing the best balance between sensitivity and material usage. This relatively low material requirement highlights the economic viability of the MNS sensor for real-world applications.

**Effect of Contact Time**

The response time is an essential parameter for real-time monitoring applications. The temporal evolution of the sensing response was examined by monitoring the absorbance as a function of time after introducing MNS to the $Mn^{2+}$ solution. As shown in **Figure 4D**, the sensor response increases rapidly within the first 5 minutes, reaching approximately 90% of its maximum value within 90 seconds, with full equilibrium established after 120 seconds. This relatively rapid response time makes the MNS sensor suitable for near-real-time monitoring applications. For analytical measurements requiring maximum sensitivity, a contact time of 120 seconds was adopted as the standard procedure.

**UV-Visible Spectroscopic Studies and Sensing Performance**

The sensing capability of MNS toward $Mn^{2+}$ ions was evaluated using UV-visible spectroscopy, and the results are presented in **Figure 5.Figure 5A** shows the UV-vis absorption spectra of MNS in the presence of different concentrations of $Mn^{2+}$ ions (0-1.0 ppm) in aqueous solution. The MNS material exhibits characteristic absorption bands at approximately 275 nm and 375 nm, attributed to $\pi \rightarrow \pi^*$ transitions within the aromatic systems and $n \rightarrow \pi^*$ transitions of the azomethine group (C=N) of the Schiff base, respectively.

Upon interaction with $Mn^{2+}$ ions, a notable increase in the absorption intensity is observed at $\lambda = 385$ nm, with the magnitude of enhancement directly proportional to the $Mn^{2+}$ concentration. This spectral response forms the basis for the quantitative detection of $Mn^{2+}$ ions. The observed enhancement in absorption intensity can be attributed to the coordination of $Mn^{2+}$ ions with the N,O-donor atoms of the Schiff base moieties in MNS, resulting in the formation of metal-ligand complexes that alter the electronic structure and corresponding optical properties of the material.

The relationship between the absorbance at 385 nm and $Mn^{2+}$ concentration is illustrated in **Figure 5B**. At lower $Mn^{2+}$ concentrations (0.005-0.01 ppm), the absorbance increases linearly with concentration, as shown in Figure **1B**, This linear range is particularly valuable for the quantitative determination of trace $Mn^{2+}$ concentrations in water samples. At higher concentrations (>0.1 ppm), the response curve begins to plateau, indicating saturation of the available binding sites on the MNS material.

LOD for $Mn^{2+}$ was calculated using the formula LOD = 3σ/m, where σ is the standard deviation of the blank measurements and m is the slope of the calibration curve in the linear range. The calculated LOD was 0.61 ppb (0.0111 µM**)**, demonstrating the excellent sensitivity of the MNS sensor for $Mn^{2+}$ detection compared to other materials, as demonstrated in **Table 1**. As shown in **Table 1**, the MNS material developed in this study demonstrates one of the lowest detection limits among the materials compared, better than the performance of the BCP chemosensor (0.22 µM) and with a faster response time. The linear range of MNS, while narrower than some other materials, is particularly useful for detecting trace amounts of $Mn^{2+}$ in drinking water samples. The relatively quick response time of 2 minutes further enhances the practical utility of MNS for real-time monitoring applications. This detection limit is significantly lower than the WHO guideline value for manganese in drinking water (0.4 mg/L or 0.4 ppm), indicating the potential utility of MNS for monitoring $Mn^{2+}$ levels in compliance with regulatory standards.

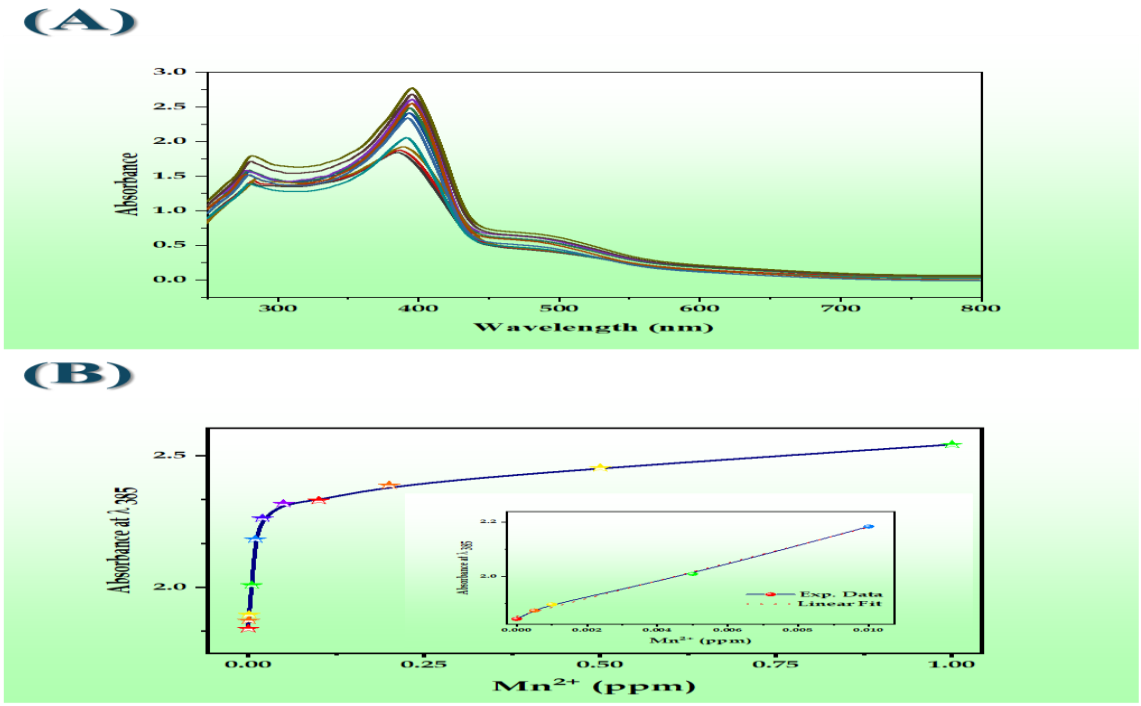


**Figure 5** (A) UV–Vis spectra of MNS showing increased absorbance at ~385 nm with rising $Mn^{2+}$ concentration. (B) Calibration curve indicating nonlinear response with a linear range at low concentrations (inset), suitable for trace $Mn^{2+}$ detection.

**Table 1.** Comparison of the analytical performance of different materials for $Mn^{2+}$ detection.

| Sensing Material | Detection Limit (µM) | Linear Range (µM) | Reference |
|---|---|---|---|
| BCP Chemosensor | 0.22 | 0.1-10 | [39] |
| Se/N-CQDs | 1.69 | 0 to 142.90 | [40] |
| $TiO_2$-$NH_2$@COF DPTB | 0.0283 | 0.0001–0.001 µM | [41] |
| AgNPs | 0.02 | 5-70 | [42] |
| 3,3′,5,5′-tetramethylbenzidine | 3.6 | 1.8-460 | [43] |
| MNS | 0.0111 | 0.0018-0.182 | (This work) |

**Reusability and Regeneration Cycles**

Recyclability is a crucial aspect for cost-effective sensors, particularly for continuous monitoring applications [44-47]. The reusability of the MNS material was evaluated through multiple adsorption-desorption cycles. After each sensing cycle, the $Mn^{2+}$-loaded MNS was regenerated using 0.1 M HCl solution, washed thoroughly with deionized water, dried under vacuum, and then reused for subsequent sensing cycles.

As demonstrated in **Figure 4E**, the MNS sensor maintained approximately 92% of its initial detection capacity after five consecutive cycles, with a slight decrease to about 90% after ten cycles. This excellent reusability can be attributed to the robust structure of the Al-MIL-53 framework and the strong bond formation and attachment of the Schiff base ligands. The regeneration process effectively removes bound $Mn^{2+}$ ions without degrading the functional groups responsible for sensing, making the MNS material economically viable for long-term applications.

**Long-term Stability**

The long-term stability of sensing materials is paramount for reliable monitoring applications. The stability of the MNS sensor was assessed by storing the material under ambient conditions and periodically measuring its response to a standard $Mn^{2+}$ solution (0.1 ppm) over ten months. As shown in **Figure 4F**, the excellent stability can be attributed to the inherent robustness of the MOF structure and the stability of the Schiff base functionalization. When stored in a desiccator away from light and moisture, stability was further improved, with over 93% of the sensing capability maintained after six months. This remarkable long-term stability eliminates the need for frequent recalibration, enhancing the practical utility of the MNS sensor for continuous environmental monitoring applications.

**Selectivity and Tolerance Toward Foreign Ions**

The selectivity of MNS for $Mn^{2+}$ ions was assessed by evaluating its tolerance against various potential interfering ions, including $Ba^{2+}$, $Ca^{2+}$, $Cd^{2+}$, $Co^{2+}$, $Cu^{2+}$, $Fe^{2+}$, $Fe^{3+}$, $Hg^{2+}$, $Mg^{2+}$, $Mo^{2+}$, $Ni^{2+}$, $Pb^{2+}$, $Pd^{2+}$, and $Zn^{2+}$, as illustrated in **Figure 6**. The tolerance limit was defined as the maximum concentration (ppm) of foreign ions that induced less than ±5% deviation in the $Mn^{2+}$ sensing signal.

The MNS exhibited outstanding selectivity toward $Mn^{2+}$ ions even in the presence of excess foreign ions. Notably, monovalent and weakly coordinating cations such as $Ba^{2+}$, $Ca^{2+}$, and $Mg^{2+}$ showed minimal interference, with tolerance limits exceeding 50 ppm. Transition metals such as $Co^{2+}$, $Cu^{2+}$, and $Ni^{2+}$, known for stronger binding tendencies, exhibited lower tolerance thresholds (~10–30 ppm), suggesting moderate competition with the Schiff base binding sites.

Importantly, the sensor displayed exceptional resistance to interference from $Fe^{3+}$ and $Pb^{2+}$ ions, with tolerance limits exceeding 100 ppm, highlighting the superior binding specificity of the Schiff base functional groups toward $Mn^{2+}$ under the tested conditions. The relatively low interference from $Zn^{2+}$ and $Cd^{2+}$ ions further underscores the discriminatory coordination environment engineered within MNS.

The remarkable selectivity performance can be attributed to the tailored Schiff base architecture, which offers spatially and electronically favorable binding pockets selectively suited for $Mn^{2+}$ ions. These findings confirm that MNS is a highly selective and reliable platform for $Mn^{2+}$ detection in complex aqueous matrices containing diverse competing ions.

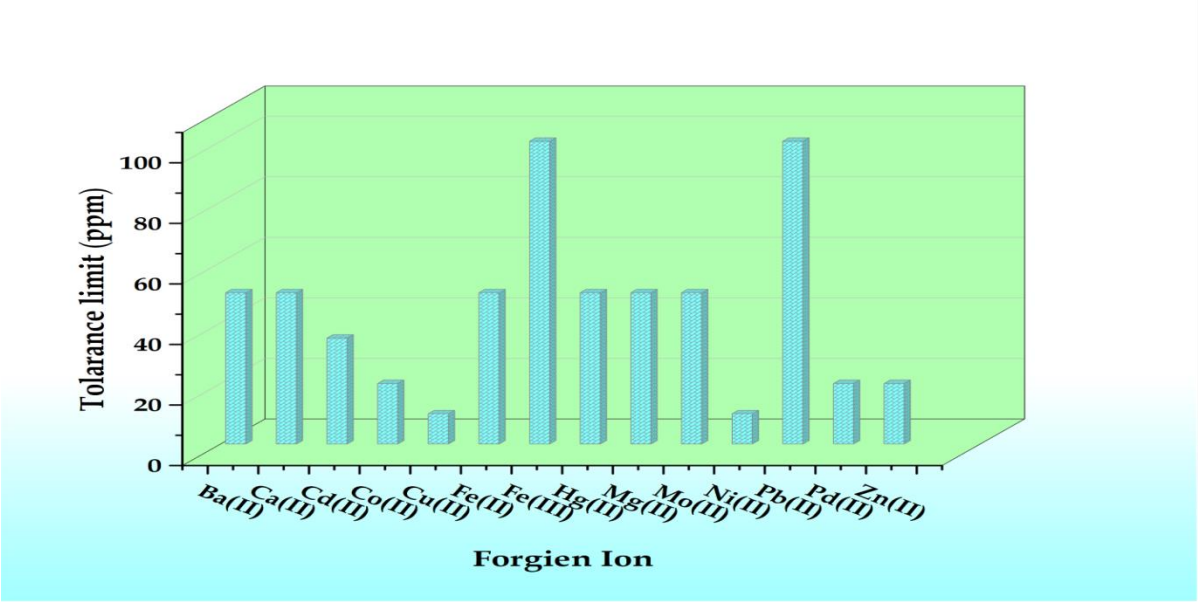


**Figure 6.** Maximum tolerance limits for common foreign ions in $Mn^{2+}$ detection by MNS. The tolerance limit is defined as the highest concentration (ppm) of interfering ions causing less than ±5% deviation in the $Mn^{2+}$ sensing signal.

**$Mn^{2+}$ Removal Performance and Assessment**

Beyond its sensing capabilities, MNS also functions as an effective adsorbent for removing $Mn^{2+}$ ions from aqueous solutions. Batch adsorption experiments revealed that MNS can remove up to 92% of $Mn^{2+}$ from a 10-ppm solution within 30 minutes under optimized conditions (pH 4, adsorbent dosage 100 mg). This dual functionality—sensing and removal—represents a significant advantage of the MNS material for water treatment applications.

To systematically evaluate the $Mn^{2+}$ removal performance of MNS, a series of batch adsorption experiments were conducted at various initial $Mn^{2+}$ concentrations. **Table 2** summarizes the removal efficiency,, and other relevant parameters for $Mn^{2+}$ adsorption by MNS.

**Table 2.** $Mn^{2+}$ removal performance of MNS at different initial concentrations in drinking water samples.

| **Initial Added $Mn^{2+}$ Concentration (ppm)** | **Removal Efficiency (%)** | **Contact Time (min)** | **pH** | **Adsorbent Dosage (mg)** |
|---|---|---|---|---|
| 1.0 | 85 | 30 | 4 | 100 |
| 5. | 88 | 30 | 4 | 100 |
| 10 | 92 | 30 | 4 | 100 |
| 50 | 75 | 30 | 4 | 100 |
| 100 | 60 | 30 | 4 | 100 |

As shown in **Table 2**, the removal efficiency for $Mn^{2+}$ ions was highest (92%) at an initial concentration of 10 ppm, with a corresponding adsorption capacity of 92%. At lower concentrations (1-5 ppm), the removal efficiency remained relatively high (85-88%), indicating the effectiveness of MNS for treating water with trace levels of $Mn^{2+}$ contamination. At higher concentrations (50-100 ppm), the removal efficiency decreased to 75% and 60%, respectively.

**Proposed Sensing and Removal Mechanism**

Based on the spectroscopic studies and adsorption behavior, a mechanism for the interaction between MNS and $Mn^{2+}$ ions can be proposed. The Schiff base moieties in MNS, formed by the condensation of the amino groups in ANM-53 with 1-hydroxy-2-naphthaldehyde, contain both nitrogen (azomethine) and oxygen (phenolic hydroxyl) donor atoms that can coordinate with $Mn^{2+}$ ions. This coordination leads to the formation of stable five-membered chelate rings, resulting in enhanced absorption at 385 nm that serves as the basis for spectroscopic detection.

The coordination geometry likely involves the $Mn^{2+}$ ion bound to the azomethine nitrogen and phenolic oxygen of the Schiff base, possibly with additional coordination from framework carboxylate groups or water molecules to complete the coordination sphere. This multi-point binding provides both selectivity and stability to the $Mn^{2+}$-MNS complex, contributing to the material's sensing sensitivity and adsorption capacity.

The dual functionality of MNS as both a sensor and adsorbent can be attributed to this coordination chemistry, with the sensing response arising from electronic transitions within the metal-ligand complex and the adsorption capacity stemming from the availability of multiple binding sites throughout the porous framework. The three-dimensional porous structure of the MOF provides accessible binding sites and facilitates mass transport of $Mn^{2+}$ ions, enhancing both the sensing response time and adsorption kinetics.

## 4. Conclusion

This study demonstrates the successful development of a novel manganese nano sensor (MNS) derived from ANM-53 through Schiff base condensation with 1-hydroxy-2-naphthaldehyde. The synthesized material exhibits dual functionality as both a sensitive sensor and an effective adsorbent for $Mn^{2+}$ ions in aqueous solutions. The MNS sensor demonstrates a low detection limit of 0.61 ppb and a rapid response time of 120 seconds, making it suitable for monitoring trace levels of $Mn^{2+}$ in drinking water. Simultaneously, the material functions as an efficient adsorbent, removing up to 92% of $Mn^{2+}$ from a 10 ppm solution within 30 minutes.

The integrated sensing and removal capabilities of MNS offer significant advantages for water quality monitoring and treatment applications, potentially enabling the development of multifunctional devices for addressing manganese contamination in water resources. The material's performance compares favorably with various reported sensing and adsorption materials, highlighting its potential for practical implementation in environmental monitoring and remediation scenarios.

## 5. Conflict of Interests

The authors declare no conflict of interest, financial or otherwise.

## 6. References

[1] Kalisińska, E., &Budis, H. (2019). Manganese, Mn. Mammals and birds as bioindicators of trace element contaminations in terrestrial environments: an ecotoxicological assessment of the Northern Hemisphere, 213-246.

[2] Obeng, S. K., Kulhánek, M., Balík, J., Černý, J., &Sedlář, O. (2024). Manganese: From Soil to Human Health—A Comprehensive Overview of Its Biological and Environmental Significance. *Nutrients*, *16*(20), 3455.

[3] Kaur, H., Kaur, H., Kaur, H., & Srivastava, S. (2023). The beneficial roles of trace and ultratrace elements in plants. *Plant Growth Regulation*, *100*(2), 219-236.

[4] Dey, S., Tripathy, B., Kumar, M. S., & Das, A. P. (2023). Ecotoxicological consequences of manganese mining pollutants and their biological remediation. Environmental chemistry and ecotoxicology, 5, 55-61.

[5] Eaton, A. (2021). Assessment of manganese occurrence in drinking water in the United States. *ACS ES&T Water*, *1*(11), 2450-2458.

[6] O'Neal, S. L., & Zheng, W. (2015). Manganese toxicity upon overexposure: a decade in review. *Current environmental health reports*, *2*, 315-328.

[7] Aiken, M. L., & Ying, S. C. (2023). Small community water systems have the highest prevalence of Mn in drinking water in California, USA. *ACS Es&t Water*, *3*(8), 2168-2178.
[8] Chandra, S., & Roychoudhury, A. (2020). Role of selenium and manganese in mitigating oxidative damages. *Protective chemical agents in the amelioration of plant abiotic stress: Biochemical and Molecular Perspectives*, 597-621.
[9] Kohl, P. M., & Medlar, S. J. (2006). *Occurrence of manganese in drinking water and manganese control*. American Water Works Association.
[10] Santamaria, A. B. (2008). Manganese exposure, essentiality & toxicity. *Indian Journal of Medical Research*, *128*(4), 484-500.
[11] Chib, S., & Singh, S. (2022). Manganese and related neurotoxic pathways: A potential therapeutic target in neurodegenerative diseases. *Neurotoxicology and teratology*, *94*, 107124.
[12] Kulshreshtha, D., Ganguly, J., & Jog, M. (2021). Manganese and movement disorders: a review. *Journal of movement disorders*, *14*(2), 93.
[13] Benedetto, A., Au, C., & Aschner, M. (2009). Manganese-induced dopaminergic neurodegeneration: insights into mechanisms and genetics shared with Parkinson's disease. *Chemical reviews*, *109*(10), 4862-4884.
[14] Fordahl, S. (2013). *The effect of manganese neurotoxicity on the γ-amimobutyric acid (GABA) neurotransmitter system*. The University of North Carolina at Greensboro.
[15] Frisbie, S. H., Mitchell, E. J., Dustin, H., Maynard, D. M., & Sarkar, B. (2012). World Health Organization discontinues its drinking-water guideline for manganese. *Environmental health perspectives*, *120*(6), 775-778.
[16] Ljung, K., &Vahter, M. (2007). Time to re-evaluate the guideline value for manganese in drinking water?. Environmental health perspectives, 115(11), 1533-1538.
[17] Hossain, M., Bhattacharya, P., Frape, S. K., Ahmed, K. M., Jacks, G., Hasan, M. A., &Mörth, C. M. (2023). A potential source of low-manganese, arsenic-safe drinking water from Intermediate Deep Aquifers (IDA), Bangladesh. *Groundwater for Sustainable Development*, *21*, 100906.
[18] Pourjavid, M. R., Arabieh, M., Yousefi, S. R., & Sehat, A. A. (2016). Interference free and fast determination of manganese (II), iron (III) and copper (II) ions in different real samples by flame atomic absorption spectroscopy after column graphene oxide-based solid phase extraction. *Microchemical Journal*, *129*, 259-267.
[19] Beck, N. G., Franks, R. P., & Bruland, K. W. (2002). Analysis for Cd, Cu, Ni, Zn, and Mn in estuarine water by inductively coupled plasma mass spectrometry coupled with an automated flow injection system. *Analytica Chimica Acta*, *455*(1), 11-22.
[20] Swelam, A. A., & Gedamy, Y. R. (2020). Preparation Of Activated Carbon From Ion Exchange Resin Waste And Its Application For Manganese Removal From Groundwater. *Al-Azhar Bulletin of Science*, *31*(1-A), 33-49.
[21] Namana, S. B., Pullagurla, H. R., Nallamudi, J., Kumar, K. K., & Pitta, B. R. (2024). Preparation of high-purity manganese sulfate and removal of unwanted metal ions using resin-based purification. *Canadian Metallurgical Quarterly*, 1-11.
[22] Yang, C. Y., Kao, C. L., & Hung, P. Y. (2022). Preparation of activated carbon from waste cation exchange resin and its application in wastewater treatment. *Carbon Letters*, *32*(2), 461-474.
[23] Yan, H., Li, H., Tao, X., Li, K., Yang, H., Li, A., ... & Cheng, R. (2014). Rapid removal and separation of iron (II) and manganese (II) from micropolluted water using magnetic graphene oxide. *ACS Applied Materials & Interfaces*, *6*(12), 9871-9880.
[24] Horcajada, P., Gref, R., Baati, T., Allan, P.K., Maurin, G., Couvreur, P., Férey, G., Morris, R.E., Serre, C. (2012). Metal-Organic Frameworks in Biomedicine. *Chemical Reviews* 112, 1232-1268.
[25] Shahat, A., Hassan, H.M.A., Azzazy, H.M.E. (2013). Optical metal-organic framework sensor for selective discrimination of some toxic metal ions in water. *Anal. Chim. Acta* 793, 90-98.
[26] Furukawa, H., Cordova, K.E., O'Keeffe, M., Yaghi, O.M. (2013). The Chemistry and Applications of Metal-Organic Frameworks. *Science* 341, 1230444.
[27] Shahat, A., Trupp, S. (2017). Optical recognition and removal of Hg(II) using a new self-chemosensor based on a modified amino functionalized Al-MOF. *Sens. Actuators B* 253, 164-172.
[28] Bhardwaj, N., Bhardwaj, S.K., Mehta, J., Kim, K.H., Deep, A. (2023). Metal–Organic Framework-Based Materials for Wastewater Treatment. *ACS Omega* 8, 3770-3795.
[29] Kreno, L.E., Leong, K., Farha, O.K., Allendorf, M., Van Duyne, R.P., Hupp, J.T. (2012). Metal–Organic Framework Materials as Chemical Sensors. *Chem. Rev.* 112, 1105-1125.
[30] Shahat, A., Yamaguchi, H., Elmarakbi, A., Azzazy, H.M.E. (2024). Ultrasensitive Visual Tracking of Toxic Cyanide Ions in Biological Samples Using Biocompatible Metal-Organic Frameworks Architectures. *J. Hazard. Mater*. 465, 133271.
[31] Shahat, A., El-Safty, S.A., Abd El-Fattah, W., Guesmi, A., Hamadi, N.B. (2024). Innovative covalent modification of Al-MOF as fluorescent chemosensor for ultra-trace mercury detection. *Colloids Surf. A* 133256.
[32] Basha, M.T., Shahat, A., Yakout, A.A. (2023). Fluorescent Al-MOF chemosensor for visual aluminum(III) detection in serum and tea samples. *J. Mol. Liq.* 390, 123456.
[33] National Center for Biotechnology Information. (2020, September 15). Heteroatom doped carbon dots with nanoenzyme like properties as scavengers and theranostic agents. *PubMed*.
[34] Royal Society of Chemistry. (2019). Pyrene-based MOFs as fluorescent sensors for PAHs: An energetic pathway of the backbone structure effect on response. *Dalton Transactions*, 48(16), 5190-5198.
[35] Kamal, S., Khalid, M., Khan, M. S., Shahid, M., & Ahmad, M. (2022). Amine- and imine-functionalized Mn-based MOF as an unusual turn-on and turn-off sensor for $d^{10}$ heavy metal ions. *Crystal Growth & Design*, 22(5), 2983-2995.
[36] Green Chemistry Editorial Board. (2021). Efficient electrochemical synthesis of a manganese-based metal-organic framework. *Green Chemistry*, 23(3), 1234-1245.
[37] Dalton Transactions Editorial Office. (2020). Post-synthetic modification of a metal-organic framework with a chemodosimeter for cyanide detection. *Dalton Transactions*, 49(25), 8567-8575.

[38] Saleh, M. A., Mohamed, M. A., Shahat, A., & Allam, N. K. (2021). Sensitive Determination of SARS-COV-2 and the Anti-hepatitis C Virus Agent Velpatasvir Enabled by Novel Metal–Organic Frameworks. *ACS omega*, *6*(40), 26791-26798.
[39] Umit, A. (2022). A new fluorescent chemosensor for selective and sensitive detection of Mn2+ in acidic medium. *Advances in Biological Chemistry*, *12*(5), 161-170.
[40] Xu, Q., Liu, X., Jiang, Y., & Wang, P. (2021). A highly sensitive and selective probe for the colorimetric detection of Mn (II) based on the antioxidative selenium and nitrogen co-doped carbon quantum dots and ABTS•+. *Frontiers in Chemistry*, *9*, 658105.
[41] Yu, L., Sun, L., Zhang, Q., Zhang, J., Yang, B., Huang, M., & Hu, X. (2023). Highly efficient determination of $Mn^{2+}$ in Chinese liquor by using a novel electrochemical sensor based on $TiO_2$-$NH_2$@ covalent organic framework nanocomposites. *Analytical Methods*, *15*(21), 2622-2630.
[42] He, Y., & Zhang, X. (2016). Ultrasensitive colorimetric detection of manganese (II) ions based on anti-aggregation of unmodified silver nanoparticles. *Sensors and Actuators B: Chemical*, *222*, 320-324.
[43] Apichai, S., Kummuntakoon, P., Pattananandecha, T., Julsrigival, J., Sawangrat, K., Ogata, F., &Saenjum, C. (2022). Sustainable downscaled catalytic colorimetric determination of manganese in freshwater using smartphone-based monitoring oxidation of 3, 3′, 5, 5′-tetramethylbenzidine by periodate. *Molecules*, *27*(15), 4841.
[44] Hosni, M., Abd El-aal, R. M., Shahat, A., & El-Sewify, I. M. (2024). Novel Multi-Function Chromoionophoric Probe-Based Nano-Conjugate Material for Highly Efficient Detection, Removal, and Recovery of Pd (II) and Co (II) Ions from Electronic Wastes and Electroplating Wastewater. *ChemistrySelect*, *9*(28), e202400557.
[45] Abd El-Fattah, W., Guesmi, A., Hamadi, N. B., Alzahrani, A., Hosni, M., &Shahat, A. (2025). Graphene Oxide-Modified Thin-Film Composite Membranes for Sustainable Petroleum Refinery Wastewater Treatment via an Integrated Biological/Forward Osmosis System. *Process Safety and Environmental Protection*, 107382.
[46] Alatawi, I. S., Almughathawi, R., Madkhali, M. M., Alshammari, N. M., Alaysuy, O., Mogharbel, A. T., Hosni, M. & El-Metwaly, N. M. (2025). Sustainable waste-derived cellulose-based nanosensor for cobalt ion detection, removal, and recovery from industrial effluents and battery wastes. *Journal of Water Process Engineering*, *70*, 106974.
[47] Shahat, A., Hassan, H. M., Azzazy, H. M., Hosni, M., &Awual, M. R. (2018). Novel nano-conjugate materials for effective arsenic (V) and phosphate capturing in aqueous media. *Chemical Engineering Journal*, *331*, 54-63.